Journal of Molecular Structure 981 (2010) 10–20

Contents lists available at ScienceDirect

Journal of Molecular Structure

journal homepage: www.elsevier.com/locate/molstruc

Experimental and theoretical study on the structure and optical properties of 2-acyl-1,3-indandiones – Conformational effects

Anife Ahmedova [a,*], Gordana Pavlović [b], Diana Zhiryakova [c], Dubravka Šišak [d], Neyko Stoyanov [e], Michael Springborg [f], Mariana Mitewa [a]

[a] Faculty of Chemistry, University of Sofia, 1, J. Bourchier av., 1164 Sofia, Bulgaria
[b] Laboratory of General Chemistry, Department of Applied Chemistry, Faculty of Textile Technology, University of Zagreb, Prilaz baruna Filipovića 28a, HR-10000 Zagreb, Croatia
[c] Institute of Organic Chemistry and Phytochemistry, Bulgarian Academy of Sciences, Acad. Bonchev str. Bl.9, Sofia 1113, Bulgaria
[d] Laboratory of Crystallography, Pliva R&D, Prilaz baruna Filipovića 29, HR-10000 Zagreb, Croatia
[e] Rousse University, Technological Branch – Razgrad, 3, Aprilsko Vastanie Str., Razgrad-7200, Bulgaria
[f] Physical and Theoretical Chemistry, University of Saarland, Saarbruecken 66123, Germany

ARTICLE INFO

Article history:
Received 29 May 2010
Received in revised form 6 July 2010
Accepted 6 July 2010
Available online 29 July 2010

Keywords:
1,3-Indandione
Optical properties
TD-DFT
Crystal structure

ABSTRACT

A series of six 2-acyl-1,3-indandione derivatives is studied by means of experimental (single crystal X-ray diffraction, NMR, electron absorption and emission spectroscopy) and theoretical methods (HF, DFT and TD-DFT). All possible tautomers and rotamers are described quantum-chemically on the basis of their structure, energy and optical properties. Although the heterocyclic substituent may easily rotate about a C–C bond, according to the calculated energies, the conformation in the most stable gas-phase optimized structures is the same as in the crystalline form. These results suggest that the intermolecular interactions are very weak compared to the intramolecular ones, like strong intramolecular hydrogen bonding and π-electron delocalization. Therefore, a good account of the experimental results was obtained theoretically by considering only the conformational modes of the isolated molecules in ground and excited states. The experimentally observed spectra of the studied series of compounds are characterized by very strong absorption in the visible region and weak fluorescence showing moderate to strong Stokes shift.

1. Introduction

The 2-substituted 1,3-indandiones have attracted an increasing interest during the last few decades due to their photophysical properties [1–5]. Very strong fluorescence was reported for 2-(pyridyl)- and 2-(quinolyl)-1,3-indandiones [6,7]. On the other hand, 2-acyl derivatives of 1,3-indandione posses intramolecular hydrogen bond and have been the subject of experimental and theoretical studies on the possible tautomeric equilibria [8–10]. The existence of Excited State Intramolecular Proton Transfer (ESIPT) was experimentally observed for 2-acetyl-1,3-indandione (2AID) and theoretically supported through quantum chemical (AM1) calculations in ground and excited singlet state [11]. The suggested fast and reversible tautomerization of 2AID gave the first clue that it should be photostable upon irradiation with UV-light. Later this has been experimentally proven, showing that 2AID and its metal complexes with Zn(II) and Cu(II) are even more photostable than some commercially available sunscreens, and therefore were proposed as promising sunscreen agents [12]. Of these reasons we have recently undertaken a detailed study of the structural, optical and complexation properties of 2AID derivatives in which the methyl group is substituted by extended π-conjugated system, i.e., 2-cinnamoyl-1,3-indandione (compound **1** in Fig. 1) [13,14].

The 1,3-indandione fragment is a very strong electron acceptor and when coupled with electron donating substituents of different strength the photophysical properties of the so-formed dipolar "push–pull" molecules can be modified [1,15]. Several studies have been devoted to excited state twisting observed in N,N-dimethylaminobenzylidene-1,3-indandione [16,17], its solid-state optical properties [18,19], and potential application of its derivatives as non-linear optical materials [20]. Recently, Sigalov et al. examined the role of inter- and intramolecular hydrogen bonding in stabilization of different conformers in solution of 1,3-indandione derivatives directly conjugated with a heterocyclic ring, such as 2-pyrrolyl-1,3-indandione [15]. The photophysical properties in the solid phase of 1,3-indandiones, conjugated with butadiene, similarly to the structures in Fig. 1, were recently studied in relation to the strong influence of the crystal packing [21].

In the current study, the structural and optical properties of a series of 2-acyl-1,3-indandiones, substituted with a heterocyclic ring and depicted in Fig. 1, were investigated by means of

* Corresponding author. Fax: +359 2 962 5438.
E-mail address: ahmedova@chem.uni-sofia.bg (A. Ahmedova).

0022-2860/$ - see front matter © 2010 Elsevier B.V. All rights reserved.
doi:10.1016/j.molstruc.2010.07.008

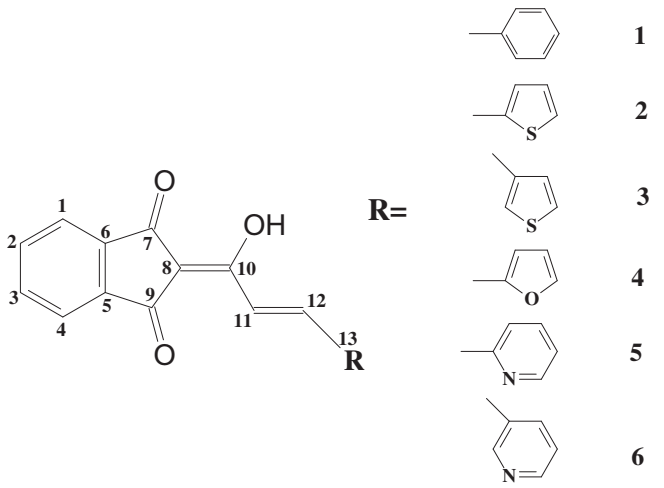

Fig. 1. Structure of the substituted 2-acyl-1,3-indandiones; compounds **1**–**6**.

experimental and theoretical methods. As can be seen, these structures allow for the formation of different keto–enol tautomers involving the 2-acyl-1,3-indandione fragment, as well as different *cis–trans* isomers in the substituted allylidene fragment. The structures were determined by X-ray diffraction and/or quantum chemical (*ab initio* and DFT) methods, whereas the optical properties were studied by UV–Vis absorption and emission spectroscopy in solution. The main question was to identify the most stable conformers in solid state and gas phase as well as the origin of the forces (intra- or intermolecular) determining their stabilization. Thus, the focus was put on the effect of the remote heterocyclic substituents on the interplay between inter- and intramolecular interactions in defining the most stable isomers and the corresponding photophysical properties.

2. Experimental

2.1. X-ray diffraction and spectroscopic experiments

Selected crystallographic and refinement data for structures **2, 3** and **4** obtained by the single crystal X-ray diffraction method are reported in Table 1. The data collection for all three structures was carried out on an Oxford Xcalibur Nova diffractometer with CCD detector and λ(Mo Kα) = 0.71703 Å for compound **2** and λ(Cu Kα) = 1.54184 Å for compounds **3** and **4**. Data collection for all structures has been performed by applying the CrysAlis Software system, Version 1.171.32.29 [22] The Lorentz-polarization effect was corrected and the intensity data reduced by the CrysAlis RED application of the CrysAlis Software system, Version 1.171.32.29 [22].

The diffraction data were scaled for absorption effects by the multi-scanning method. Both structures were solved by direct methods and refined on F^2 by weighted full-matrix least squares. Programs SHELXS97 [23] and SHELXL97 [23] integrated in the WinGX software system [24] were used to solve and refine the structures. All non-hydrogen atoms were refined anisotropically.

Hydrogen atoms were placed in geometrically idealized positions [Csp^2–H 0.93 Å with U_{iso} (H) = 1.2 U_{eq} (C)] and were constrained to ride on their parent atoms by using the appropriate SHELXL97 HFIX instructions. The hydrogen atom from the hydroxyl group was also found in difference Fourier maps at distances 0.86(5) and 0.97(2) Å in **3** and **4,** respectively and was refined freely. The molecular geometry calculations and drawings were performed by ORTEP-3, [25] PLATON [26] and Mercury [27]. The main geometrical features along with hydrogen bond geometry and π–π stacking interactions for structures **2**, **3** and **4** are given in Tables 2 and 3.

The IR spectra were recorded on a Specord 75-IR (Carl-Zeiss, Jena, Germany) in Nujol mulls. The UV–Vis absorption spectra were recorded on a JASCO V-570-UV/Vis/NIR. Fluorescence spectra were obtained in three different solvents using Perkin–Elmer LS-5 and Varian Eclipse fluorometers. All solvents were spectroscopic grade and were used without further purification. Acetonitrile was dried over P_2O_5 and freshly distilled before use. The NMR spectra were recorded in $CDCl_3$ using a Bruker DRX-250 spectrometer operating at 250.13 MHz for ^{1}H- and 62.90 MHz – for the ^{13}C-nuclei. The chemical shifts are related to TMS used as reference. NMR spectra of compounds **5** and **6** were not recorded due to very low solubility in most of the available solvents ($CDCl_3$, DMSO-d_6 or CD_3CO).

2.2. Synthesis and characterization

Compounds **1**–**6** were obtained by refluxing 4.7 g (0.025 mol) 2-acetyl-1,3-indandione, 0.05 mol of the corresponding aldehyde (**1** – benzaldehyde, **2** – thiophene-2-aldehyde, **3** – thiophene-3-aldehyde, **4** – furan-2-aldehyde, **5** – pyridine-2-aldehyde, **6** – pyridine-3-aldehyde) and 0.012 mol piperidine for 1 h. To the formed polycrystalline precipitate 50 mL of ethanol was added and the reaction mixture was boiled for a half hour more. After cooling down the formed crystals were filtered off and repeatedly washed with ethanol. The filtrate was further diluted with water, acidified and the additionally formed amount of the product was collected. The total amount of the products were recrystalized from ethanol.

Compound 1; *2-(1-hydroxy-3-phenyl-allylidene)-2H-inden-1,3-dione,* Yield 70%, M.p. 186–187 °C. Anal. Found, %: C, 78.09; H, 4.50. $C_{18}H_{12}O_3$; Calcd, %: C, 78.25; H, 4.38. **IR** (Nujol) ν, cm^{-1}: broad >3200 (ν_{O-H}), 1700 ($\nu_{C=O}$), 1650 ($\nu_{C=O}$, $\nu_{C=C}$), 1610 ($\nu_{C=O}$, $\nu_{C=C,\ (Ph)}$), 1585 ($\nu_{C=C,\ (Ph)}$), 1550 ($\nu_{C=C,\ (Ph)}$), 1290 (δ_{OH}), 1135 (δ_{CH}), 980 ($\gamma_{=C-H}$), 750 (γ_{Ar-H}). ^{1}H NMR ($CDCl_3$), δ, ppm: 13.15 (s, 1H), 7.85–8.00 (m, 2H), 7.64–7.73 (m, 4H), 7.4–7.42 (m, 5H). ^{13}C NMR ($CDCl_3$), δ, ppm: 197.4 (C7), 188.5 (C9), 173.1 (C10), 144.8 (C11), 141.0 (C6), 138.7 (C5), 134.9 (C2), 134.7 (C3), 134.0 (C13), 131.1 (C12), 129.0 (C17, C15), 129.0 (C18, C14), 122.6 (C1), 122.3 (C4), 117.9 (C16), 107.8 (C8).

Compound 2; *2-(3-thiophen-2-yl-1-hydroxy-allylidene)-2H-inden-1,3-dione,* Yield 45%; M.p. 172–173 °C. Anal. Found, %: C, 68.47; H, 3.89; S, 12.48. $C_{16}H_{10}O_3S$. Calcd, %: C, 68.07, H, 3.57, S, 11.36. IR (Nujol) ν, cm^{-1}: 3400 broad (ν_{O-H}), 1700 ($\nu_{C=O}$), 1650 ($\nu_{C=O}$, $\nu_{C=C}$), 1605 ($\nu_{C=O}$, $\nu_{C=C,\ (Ph)}$), 1590 ($\nu_{C=C,\ (Ph)}$), 1555 ($\nu_{C=C,\ (Ph)}$), 1500 ($\nu_{C=C,\ (Ph)}$), 1400 ($\nu_{C=C,\ (Ph)}$), 1295 (δ_{OH}), 1135 (δ_{CH}), 980 ($\gamma_{=C-H}$), 750 (γ_{Ar-H}). ^{1}H NMR ($CDCl_3$), δ, ppm: 11.9 (s, 1H), 7.91–7.58 (H, arom), 7.57–7.31 (m, 3H), 7.20–6.97 (m, 2H). ^{13}C NMR ($CDCl_3$), δ, ppm: 197.2 (C7), 188.3 (C9), 172.6 (C10), 140.8 (C6), 140.5 (C5), 138.6 (C13), 137.1 (C11), 134.7 (C2), 133.9 (C3), 132.4 (C12), 130.8 (C14), 128.5 (C16), 122.4 (C1), 122.1 (C4), 116.4 (C15), 107.4 (C8).

Compound 3; *2-(3-thiophen-3-yl-1-hydroxy-allylidene)-2H-inden-1,3-dione,* Yield 65%; M.p. 193–194 °C. Anal. Found, %: C, 68.29; H, 3.93; S, 13.40. $C_{16}H_{10}O_3S$. Calcd, %: C, 68.07; H, 3.57; S, 11.36. IR (Nujol) ν, cm^{-1}: 3400 broad (ν_{O-H}), 1700 ($\nu_{C=O}$), 1625 ($\nu_{C=O}$, $\nu_{C=C}$) 1605 ($\nu_{C=O}$, $\nu_{C=C}$) 1580 ($\nu_{C=O}$, $\nu_{C=C,\ (Ph)}$), 1570 ($\nu_{C=O}$, $\nu_{C=C,\ (Ph)}$), 1550 ($\nu_{C=O}$, $\nu_{C=C,\ (Ph)}$), 1320 (ν_{N-Ar}), 1285 (δ_{OH}), 1150 (δ_{CH}), 985 ($\gamma_{=C-H}$), 820 (γ_{Ar-H}), 780 (γ_{Ar-H}). ^{1}H NMR ($CDCl_3$), δ, ppm: 12.15 (s, ^{1}H), 7.76–7.61 (m, 4H), 7.56–7.45 (m, 2H), 7.44–7.33 (m, 3H). ^{13}C NMR ($CDCl_3$), δ, ppm: 197.4 (C7), 188.6 (C9), 173.5 (C10), 140.9 (C6), 138.7 (C5), 138.3 (C13), 138.2 (C11), 134.8 (C2), 134.0 (C3), 130.3 (C12), 127.3 (C14), 125.7 (C15), 122.6 (C1), 122.2 (C4), 117.6 (C16), 107.5 (C8).

Compound 4; *2-(3-furan-2-yl-1-hydroxy-allylidene)-2H-inden-1,3-dione,* Yield 86%; M.p. 217–218 °C. Anal. Found, %: C, 72.5; H,

Table 1
Summary of data collection and structure refinement details for compounds **2**, **3** and **4**.

Compound	**2**	**3**	**4**
Formula	$C_{16}H_{10}O_3S$	$C_{16}H_{10}O_3S$	$C_{16}H_{10}O_4$
M_r	282.30	282.300	266.24
Crystal system, colour and habit	Orthorhombic, orange plates	Orthorhombic, red–orange plates	Monoclinic, red–orange plates
Space group[a]	*P n a* 2_1	*P n a* 2_1	*P* $2_1/c$
Crystal dimensions (mm)	0.60 × 0.30 × 0.20	0.47 × 0.29 × 0.24	0.22 × 0.14 × 0.08
Unit cell parameters			
a (Å)	23.260(3)	27.2298(5)	11.8206(2)
b (Å)	4.7307(6)	3.8827(1)	3.8600 (1)
c (Å)	12.0110(14)	12.3329(2)	27.3872(4)
β (°)	–	–	101.25(1)
V (Å^3)	1321.7(3)	1303.90(5)	1225.58(4)
Z	4	4	4
D_c (g cm^{-3})	1.419	1.438	1.443
T (K)	296	296	296
μ (mm^{-1})	0.248	2.248	0.868
F (0 0 0)	584	584	552
θ Range for data collection (°)	4–28	5–73	3–73
h, *k*, *l* range	−10 to 30, −6 to 5, −14 to 15	−33 to 32, −3 to 4, −15 to 12	−14 to 14, −4 to 4, −33 to 33
Scan type	*ω*	*ω*	*ω*
No. measured reflections	4438	3453	10,736
No. independent reflections (R_{int})	2523 (0.0420)	1873 (0.0285)	2424 (0.0325)
No. observed reflections, $I \geqslant 2\sigma(I)$	1127	1815	2158
No. refined parameters/restraints	194/1	185/1	185/0
g_1, g_2 in *w*	0.0321, 0.000	0.0972, 0.0414	0.0913, 0.0965
R, *wR* [$I \geqslant 2\sigma(I)$]	0.049, 0.0719	0.0432, 0.1168	0.0452, 0.1246
R, *wR* [all data]	0.0918,0.1513	0.0443, 0.1185	0.0497, 0.1291
Goodness of fit on F^2, *S*	0.898	1.056	1.032
Max., min. electron density (e Å^{-3})	0.231, −0.135	0.205, −0.163	0.207, −0.231
Maximum Δ/σ	<0.001	<0.001	0.001

[a] Flack parameter for **3**: 0.06(2).

Table 2
Selected interatomic distances (Å) and valence angles (°) for the compounds **2**, **3** and **4** obtained from X-ray data and B3LYP/6-31G** optimizations.

	2		**3**		**4**	
	X-ray data	B3LYP/6-31G**	X-ray data	B3LYP/6-31G**	X-ray data	B3LYP/6-31G**
Bond distances						
O1–C9	1.229(4)	1.225	1.219(3)	1.226	1.2119(17)	1.225
O2–C7	1.244(5)	1.244	1.251(3)	1.243	1.2403(17)	1.244
O3–C10	1.338(4)	1.332	1.335(3)	1.331	1.3369(17)	1.333
C7–C8	1.456(6)	1.454	1.446(3)	1.454	1.4443(18)	1.454
C8–C9	1.438(6)	1.472	1.469(3)	1.472	1.4726(18)	1.473
C8–C10	1.367(6)	1.390	1.378(3)	1.390	1.3829(19)	1.390
C10–C11	1.428(6)	1.442	1.435(3)	1.444	1.4274(19)	1.442
C11–C12	1.337(6)	1.357	1.342(3)	1.354	1.348(2)	1.357
C12–C13	1.441(6)	1.437	1.439(3)	1.449	1.422(2)	1.429
Bond angles						
C2–C1–C6	117.0(6)	117.8	117.6(3)	117.8	118.04(13)	117.8
C1–C2–C3	120.9(5)	120.9	121.3(2)	120.9	121.07(13)	120.9
C2–C3–C4	121.9(6)	121.0	120.1(3)	121.0	120.84(13)	121.0
C3–C4–C5	117.5(5)	117.9	118.4(3)	117.9	118.08(12)	117.9
C4–C5–C6	122.1(4)	121.1	121.2(2)	121.0	121.11(11)	121.0
C1–C6–C5	120.7(5)	121.3	121.3(3)	121.3	120.85(12)	121.3

3.7. $C_{16}H_{10}O_4$. Calcd, %: C, 72.18; H, 3.79. IR (Nujol) *ν*, cm^{-1}: 3400–3500 broad (ν_{O-H}), 1700 ($\nu_{C=O}$), 1645 ($\nu_{C=O}$, $\nu_{C=C}$), 1615 ($\nu_{C=O}$, $\nu_{C=C}$), 1590 ($\nu_{C=O}$, $\nu_{C=C,\ (Ph)}$), 1530 ($\nu_{C=O}$, $\nu_{C=C,\ (Ph)}$), 1280 (δ_{OH}), 1150 (δ_{CH}), 985 ($\gamma_{=C-H}$), 850 (γ_{Ar-H}). ^{1}H NMR ($CDCl_3$ + DMSO-d_6), *δ*, ppm: 11.15 (s, 1H), 7.74–7.5 (m, 4H), 6.76–6.75 (m, 3H), 6.49–6.5 (m, 2H). ^{13}C NMR ($CDCl_3$ + DMSO-d_6), *δ*, ppm: 196.5 (C7), 187.6 (C9), 172.0 (C10), 150.9 (C13), 145.8 (C16), 140.3 (C6), 138.0 (C5), 134.3 (C3), 133.5 (C2), 129.8 (C12), 121.9 (C1), 121.5 (C4), 117.0 (C11), 114.6 (C14), 112.6 (C15), 106.9 (C8).

Compound 5; *2-(3-pyridin-2-yl-1-hydroxy-allylidene)-2H-inden-1,3-dione,* Yield 79%; M.p. 221–222 °C. Anal. Found, %: C, 74.05; H, 4.39; N, 5.18. $C_{17}H_{11}O_3N$. Calcd, %: C, 73.64; H, 4.00; N, 5.05. IR (Nujol) *ν*, cm^{-1}: 3450 broad (ν_{O-H}), 2500–2600 ($\nu_{C=N}$), 1690 ($\nu_{C=O}$), 1675 ($\nu_{C=O}$, $\nu_{C=C}$), 1650 ($\nu_{C=O}$, $\nu_{C=C}$), 1630 ($\nu_{C=O}$, $\nu_{C=C,\ (Ph)}$), 1585 ($\nu_{C=O}$, $\nu_{C=C,\ (Ph)}$), 1575 ($\nu_{C=O}$, $\nu_{C=C,\ (Ph)}$), 1280 (δ_{OH}), 1150 (δ_{CH}), 975 ($\gamma_{=C-H}$).

Compound 6; *2-(3-pyridin-3-yl-1-hydroxy-allylidene)-2H-inden-1,3-dione,* Yield 85%; M.p. 234–235 °C. Anal. Found, %: C, 73.60; H, 4.48; N, 5.16. $C_{17}H_{11}O_3N$. Calcd, %: C, 73.64, H, 4.00; N, 5.05. IR (Nujol) *ν*, cm^{-1}: 3500 broad (ν_{O-H}), 1700 ($\nu_{C=O}$), 1650 ($\nu_{C=O}$, $\nu_{C=C}$), 1630 ($\nu_{C=O}$, $\nu_{C=C}$), 1595 ($\nu_{C=O}$, $\nu_{C=C,\ (Ph)}$), 1580 ($\nu_{C=O}$, $\nu_{C=C,\ (Ph)}$), 1545 ($\nu_{C=O}$, $\nu_{C=C,\ (Ph)}$), 990 ($\gamma_{=C-H}$), 835 (γ_{Ar-H}).

2.3. Quantum-chemical calculations

The quantum-chemical calculations were performed with full geometry optimization without any symmetry restrictions. The potential energy surface for all studied compounds was searched for

Table 3
Hydrogen bond geometry and geometrical parameters of π–π interactions (Å, °) in the crystal structures of compounds **2**, **3** and **4**.

D–H···A	D–H	H···A	D···A	∠H···A	Symmetry code
2					
O3–H3O···O2	0.82	1.89	2.629(5)	149	–
C3–H3···O2	0.93	2.618	3.393(7)	141(1)	$-x+1/2+1,+y+1/2,+z-1/2$
C14–H14···O1	0.93	2.689	3.324(6)	126(1)	$-x+1,-y+1,+z+1/2$
3					
O3–H3O···O2	0.86(5)	1.83(5)	2.650(3)	162(5)	–
C3–H3···O2	0.93	2.676	3.417(4)	137(1)	$-x+1/2,+y-1/2,+z-1/2$
C14–H14···O1	0.93	2.550	3.246(4)	132	$1-x,2-y,1/2+z$
C15–H15···O2	0.93	2.746	3.520(4)	141(1)	$-x+1,-y+1,+z-1/2$
4					
O3–H3O···O2	0.97(2)	1.73(2)	2.629(2)	153(2)	–
C16–H16···O1	0.93	2.510	3.216(2)	133	$1-x,-y,1-z$
C14–H14···O2	0.93	2.859	3.770(2)	166(1)	$-x,-y+1,-z+1$
C2–H2···O2	0.93	2.789	3.475(2)	131(1)	$-x,+y-1/2,-z+1/2+1$
Interaction[a]	C_g–C_g distance	C_g···P1[b]	C_g···P2[c]	β[d]	Slippage
3					
$C_g(2)\cdots C_g(3)^i$	3.792(2)	3.479(1)	3.495(1)	22.85	1.473
4					
$C_g(2)\cdots C_g(3)^i$	3.638(1)	3.500(1)	3.524(1)	14.36	0.902

Symmetry code: $i = x, 1+y, z$. $C_g(2)$: centroid of cyclopentane plane in **3** and **4**. $C_g(3)$: centroid of benzene plane in **3** and **4**.
[a] The dihedral angle between planes which define the centroids $C_g(2)$ and $C_g(3)$ is 0.72(14)° in **3** and 1.55(7)° in **4**.
[b,c] C_g···P1 (or P2) is the perpendicular distance of corresponding centroid to a plane. Planes P1 or P2 are defined by the atoms, which define the corresponding centroids.
[d] β is the angle between $C_g\cdots C_g$ vector and vertical line on corresponding plane.

stable conformers. Geometries of six to eight possible rotamers and tautomers were optimized by the semiempirical AM1 and *ab initio* Hartree–Fock methods. Vibrational frequencies and intensities were computed at the same level of theory as used for the structure optimization in order to confirm that local energy minima were attained. Selected structures were further optimized using the density functional theory (DFT) and the hybrid B3LYP functional [28,29]. For all calculation the 6-31G** basis set was used. At the equilibrium geometries of the stable conformers vertical excitation energies were calculated employing ZINDO and time-dependent DFT (TD-DFT) with the above mentioned functional and basis set. TD-DFT was also applied in combination with IEF-PCM to account for the solvent effect. All calculations were carried out using the Gaussian 03 program package [30]. Supplementary material contains the energy diagrams of the calculated isomers/tautomers of compounds **1**–**6** and a complete list of the obtained total energies (in a.u. and kcal/mol) and zero-point vibrational energies.

3. Results and discussion

3.1. Theoretical calculations

From a structural point of view, the studied series of compounds allow two different kinds of intramolecular rearrangements: intramolecular proton transfer, i.e. tautomerization, and *cis–trans*-isomerizations. Of simplicity, we will call the exo- and endo-cyclic enolized forms tautomers **a** and **b**, respectively. As far as the C–C bond rotations are concerned, we shall study isomerizations via the single C10–C11 and C12–C13 bond rotations. A rotation about C10–C11 bond leads to the *s-cis* and *s-trans* isomers, and rotation about C12–C13 bond affects the orientation of the heterocyclic substituent (see Figs. 1 and 2). We found that in all optimized structures the C11–C12 double bond has *trans*-orientation of the H-atoms. (The structures and energies of *cis*-isomers were computed for the more stable tautomer and showed much higher energies and therefore were not considered further.) The most stable structures obtained from HF/6-31G** and B3LYP/6-31G** optimizations are depicted in Fig. 2. It can be seen that both methods predict that the exocyclic enolic tautomers **a**, of the *s-trans* isomers, are energetically the most favorable ones. Energy diagrams of all optimized conformers for each compound are presented in Supplementary material. The calculated relative stabilities of the possible isomers of compounds **1**–**6** are estimated on the basis of ZPVE-corrected electronic energies. (Inclusion of the zero-point vibrational energy (ZPVE) corrections do not change the energy order of the studied isomers, as could be seen from Table SM1 in the Suppl. Mater.) In summary, the calculations show that the energy differences between the **a** and **b** tautomers are *ca.* 4.0 kcal/mol (varying from 4.04 for **4** and **5** to 3.94 kcal/mol for **6**) according to DFT and *ca.* 5.0 kcal/mol according to HF data. A rotation about the C10–C11 single bond leads to *s-cis* isomer that, according to the DFT calculations, have energies that are 2.3–4.6 kcal/mol higher than those of the most stable structures, and even 4.1–6.2 kcal/mol according to the HF calculations. Also interesting is the orientation of the heterocyclic ring, i.e. the C12–C13 bond rotation. As can be seen from Fig. 2, the thiophene and furan substituents in compounds **2**, **3** and **4** are oriented so that the heterocyclic double bond position leads to a *s-trans* configuration of the C12–C13 bond, too. In this way *all s-trans* configuration, regarding the configuration of the single C10–C11 and C12–C13 bonds, is realized. A similar trend can be identified for the structures **5** and **6**, although here deviations occur due to strong delocalization in the pyridine ring. Nevertheless, the hetero-atom in compound **5** is directly bonded to C13 and is positioned closer to the 1,3-indandione fragment, similarly to structures **2** and **4**. Compounds **3** and **6** are positional isomers of **2** and **5**, respectively, and this affects the orientation of the heterocyclic substituents as can be seen in Fig. 2. The orientation of the heterocyclic rings raises the question about the role of intra- and/or intermolecular forces for stabilization of different rotamers.

It is interesting to note that the energy of the isomeric forms that result from rotating the heterocyclic substituents about the C12–C13 bond is less than 1 kcal/mol higher than the most stable structures in Fig. 2. The largest energy difference between these rotamers is obtained for compound **3** (0.97 and 1.26 kcal/mol according to DFT and HF calculations, respectively) and the small-

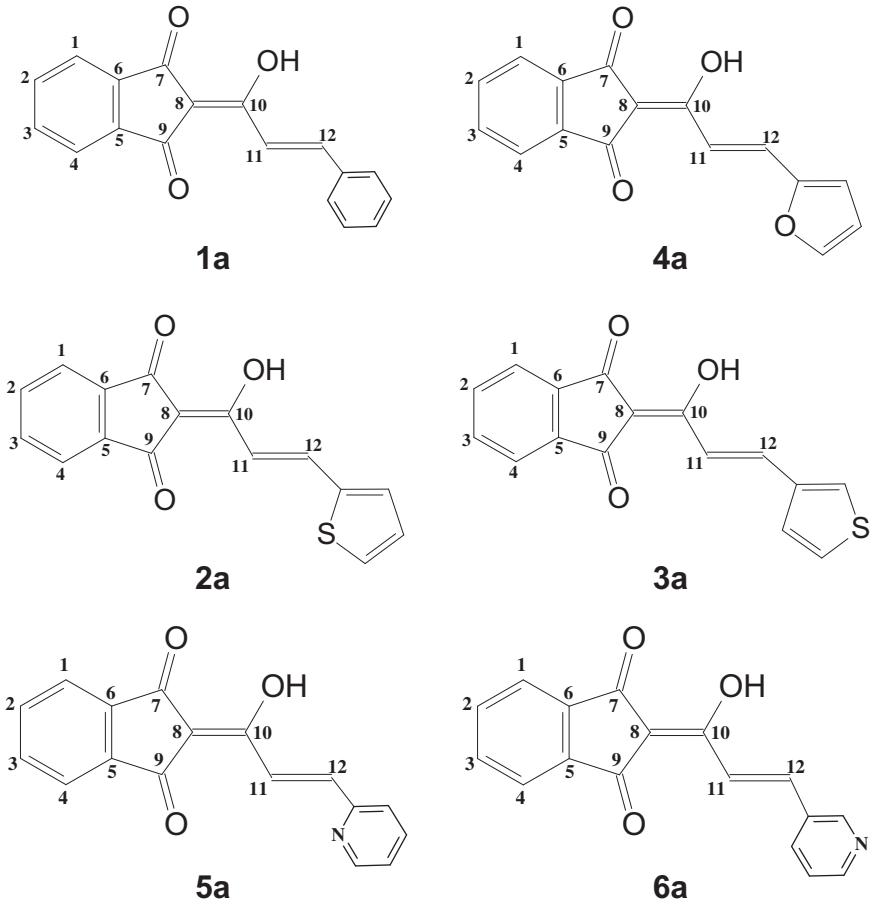

Fig. 2. Structures of the most stable conformers of compounds **1–6,** according to the HF/6-31G** and B3LYP/6-31G** calculations.

est one is for compound **5** (0.36 and 0.12 kcal/mol according to DFT and HF calculations, respectively). This implies that rotation of the heterocyclic substituent about C12–C13 bond easily can result from external factors like temperature, light, solvents, etc. In an attempt to identify a structural parameter that could possibly reflect the relative energies of the discussed rotamers it was noted that the DFT-optimized C12–C13 bond length is shorter by 0.003 Å in the most stable rotamers in compounds **2**, **3** and **4** and only by 0.001 Å in compound **5**. This might influence the degree of electron delocalization in the molecule leading to stabilization of the corresponding rotamer. Another interesting fact is that the crystal structures of compounds **2**, **3** and **4**, described further below, agree very well with the results of the isolated molecule gas-phase optimizations (HF/6-31G** and B3LYP/6-31G**) predicting the same conformation as those obtained in the crystals. The same holds for the structure of compound **6**, which was solved from powder diffraction [31]. Selected optimized structural parameters are compared with the experimental ones in Table 2.

3.2. Crystal structure descriptions of compounds 2, 3 and 4

The molecular structures of compounds **2**, **3** and **4** are depicted in Figs. 3a, 4a and 5a, respectively. All compounds are planar in the crystalline state and are in a *trans* configuration regarding the spatial orientation of the substitutents at C11=C12 double bond. The planarity of the molecules is indicated by the dihedral angle value of 6.35(17)° and 5.35(14)° between 1,3-indandione fragment and thiophene plane in **2** and **3**, respectively, and 3.12(9)° between 1,3-indandione fragment and furan plane in **4**.

Planarity of 1,3-indandione moiety in the molecules is confirmed by the dihedral angle values of 1.1(2)°, 0.72(14)° and 1.55(7)° between the planes of the benzene and cyclopentane rings in **2**, **3** and **4**, respectively. The keto oxygen atoms O1 and O2 are 0.006(3) and −0.039(3) Å in **2**, −0.002(2) and −0.002(3) Å in **3** and 0.013(1) and −0.010(1) Å in **4** apart of the cyclopentane ring plane. The geometry of the fused benzene ring with saturated five-membered ring in indane fragment of the molecule is affected so that the bonds at C1 and C4 are shortened (C1–C6 1.397(8) Å, C4–C5 1.357(7) Å in **2**, (C1–C6 1.380(3) Å, C4–C5 1.373(4) Å in **3** and C1–C6 1.386(2) Å, C4–C5 1.384(2) Å in **4**). The corresponding bond angles decrease and are less than 120° (C2–C1–C6 117.0(5)° and C3–C4–C5 117.4(5)° in **2**, C2–C1–C6 117.6(3)° and C3–C4–C5 118.4(3)° in **3** and C2–C1–C6 118.04(13)° and C3–C4–C5 118.08(12)° in **4**). The shortening of those bonds is accompanied with the elongation of the others within the benzene ring.

The β-diketone fragment is characterized by the existence of a resonance-assisted intramolecular hydrogen bond (RAHB) [32,33] O3–H3O···O2 whose geometry (O···O distance about 2.6 Å and O–H···O angle in the range 150–160°; Table 3) is as expected for RAHB due to the presence of the enol form. The RAHB forms well recognizable supramolecular synthon described by the graph-set analysis as the S(6) type. The geometry of the RAHB is not influenced by the type of the substituent *i.e.* thiophene or furan ring in **2**, **3** and **4**, respectively.

The participation of the keto O2–C7 group in the RAHB formation influences the O2–C7 bond length (the bond is elongated) in comparison with the keto O1–C9 bond length (O1–C9 1.229(6) Å and O2–C7 1.244(7) Å in **2**, O1–C9 1.219(3) Å and O2–C7

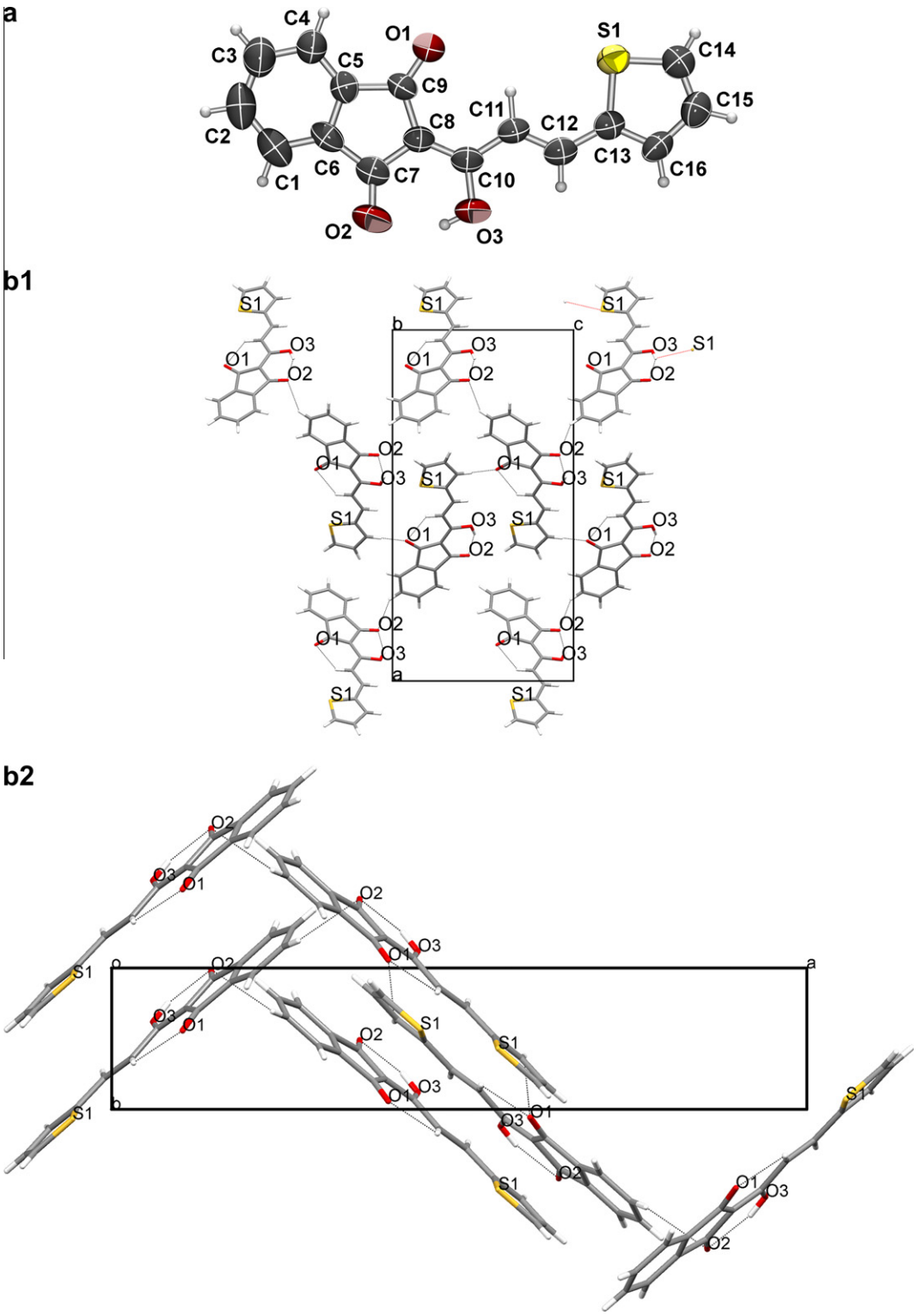

Fig. 3. ORTEP drawing of compound **2** including the atom numbering scheme. The thermal ellipsoids are drawn at the 50% probability level at 296 K (3a); the packing of molecules in *ac* plane and herringbone mode of packing of molecules in **2** viewed in *ab* plane (3b).

1.251(3) Å in **3** and O1–C9 1.212(2) Å and O2–C7 1.240(2) Å in **4**). On the contrary, the O3–C10 bond in **2**, **3** and **4** (1.338(5), 1.335(3) Å and 1.337(2) Å, respectively; Table 2), has a character of σ C*ar*–OH bond as those found in phenols [34]. Such a molecular geometry of the β-diketone fragment in **2**, **3** and **4** is in agreement with what is found in similar 1,3-indandione and indan-1-one derivatives like the 2-pivaloyl-1,3-indandione structure [35], 2-acetyl-1,3-indandione [36], 2-(hydroxy(amino)methylidene)-1,3-indandione [9] and 2-acylindan-1-one [37].

The geometry of allylidene moiety is characterized by π-electron delocalization through C–C single and double bonds (C8–C10 and C11–C12 bond lengths are 1.366(7) Å and 1.337(7) Å in

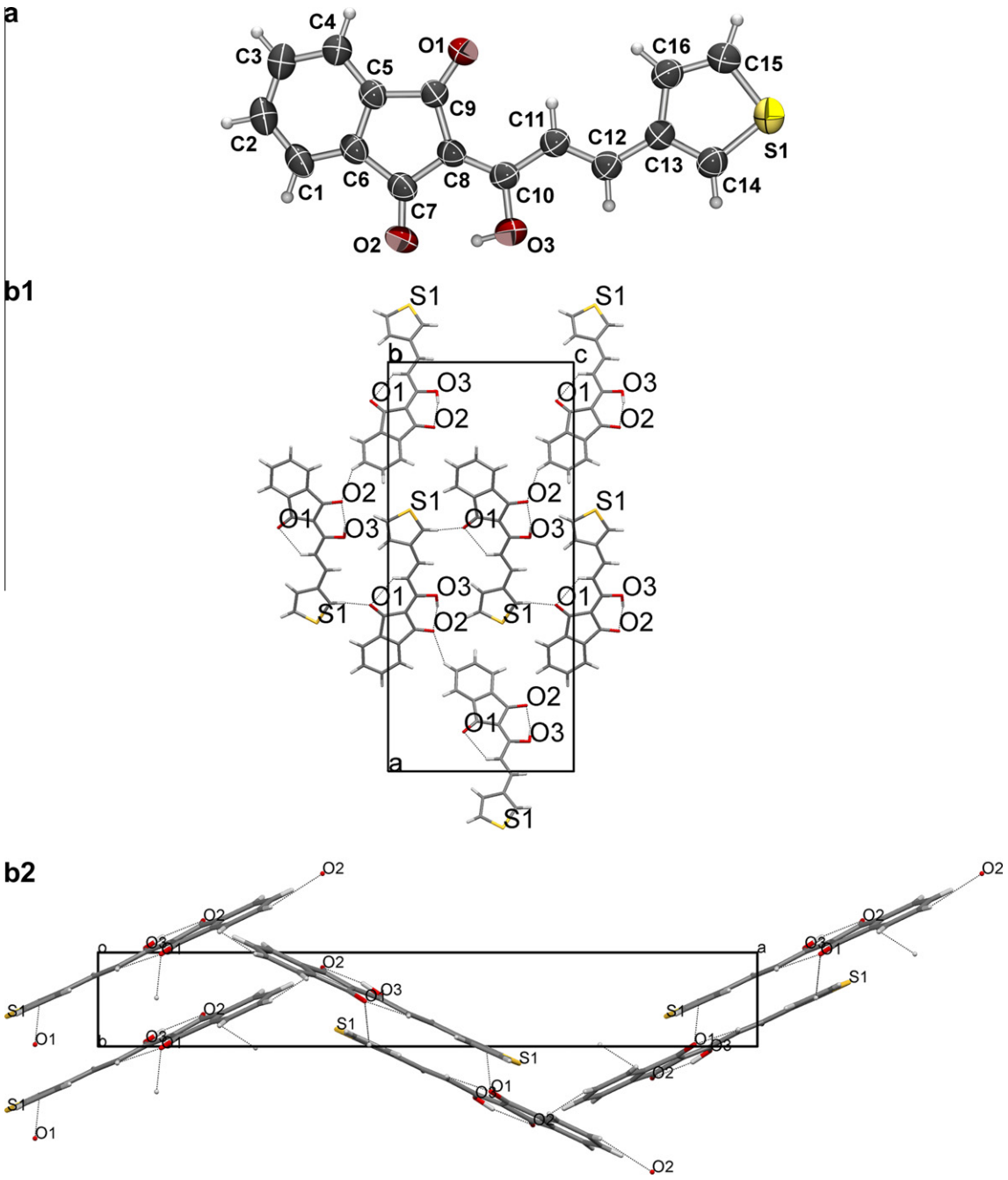

Fig. 4. ORTEP drawing of compound **3** including the atom numbering scheme. The thermal ellipsoids are drawn at the 50% probability level at 296 K (4a); the packing of molecules in *ac* plane and herringbone mode of packing of molecules **3** viewed in *ab* plane (4b).

2, 1.378(3) Å and 1.342(3) Å in **3** and 1.383(2) Å and 1.348(2) Å in **4**, while C10–C11 and C12–C13 bond lengths are 1.428(6) Å and 1.442(6) Å in **2**, 1.435(3) Å and 1.439(3) Å in **3** and 1.427(2) Å and 1.422(2) Å in **4**) (Table 2).

The compounds **2** and **3** are isostructural on the basis of similarities of molecular geometry, morphological accordance, resemblance of unit cell parameters (Table 1) and intermolecular interactions in their crystal structures (Table 3, Figs. 3b and 4b). The keto O1 atom in **2** and **3** participate in intermolecular hydrogen bond formation with the thiophene C–H group (C14–H14) (Table 3) thus forming infinite *zig-zag* chains along the *b* axis. The molecules are arranged in a herringbone fashion in *ab* plane which enables antiparallel molecular stacking (Figs. 3b and 4b). An exception is compound **4**. Here, the discrete centrosymmetric dimers are formed *via* C16–H16···O1 intermolecular hydrogen bond (Table 3). The dimers form 20-membered rings with two donor and two acceptor groups, which according to a graph-set analysis can be described as $R_2^2(20)$ (Fig. 5b).

Moreover, π–π stacking geometry in **3** and **4** (Table 3) reveal that considerable π-overlap exists between the 1,3-indandione fragments of two adjacent molecules shifted along the shortest *b* axis (Table 3, symmetry code: *x*, 1 + *y*, *z*). Almost ideal slippage is found in **3** (Table 3). Interestingly, *b* axis in **2** is also the shortest one, but longer to some extent (Table 1) than in **3** and **4** and π–π aromatic stacking with reasonable geometry is not found in **2** (the shortest slippage is about 2 Å). The criteria for π–π aromatic

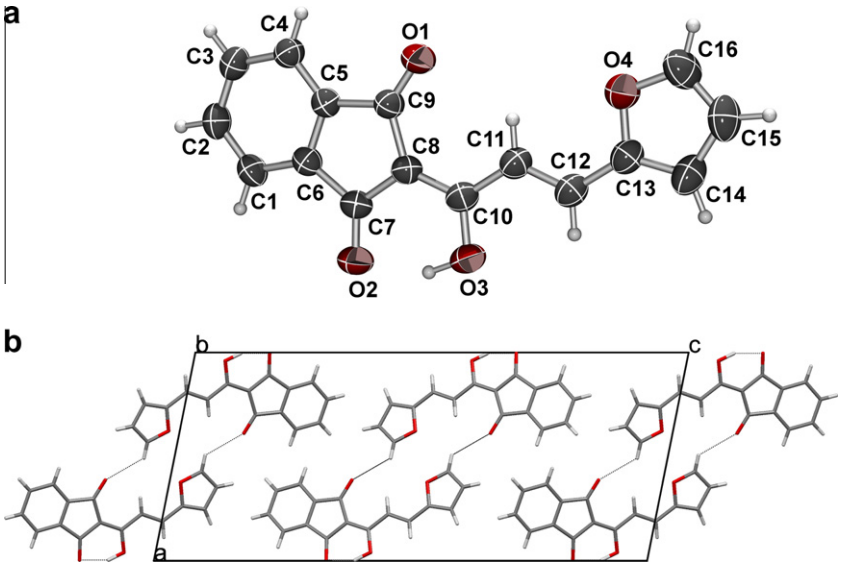

Fig. 5. ORTEP drawing of compound **4** including the atom numbering scheme. The thermal ellipsoids are drawn at the 50% probability level at 296 K (5a); centrosymmetric discrete dimers as a packing mode of molecules **4** viewed down *b* axis (5b).

stacking geometry is based on the following values: perpendicular distance between the corresponding centroids of two planes no longer than 3.8 Å (3.3–3.8 Å; C_gP1 and C_gP2) and dihedral angles (between P1 and P2) no larger than 20° [38–40]. The calculated slippage on the basis of $C_g\cdots C_g$ distances as well as the value of the angle between C_g...C_g vector and vertical line on corresponding plane has been taken into account as one of the geometrical criteria, too (approx. 1.5 Å for π–π stacking interactions).

3.3. Optical properties

Absorption spectra of all compounds in different solvents were recorded at room temperature. The data are summarized in Table 4 and compared with the calculated values for the vertical excitation energies for the most stable conformers of compounds **1**–**6** (shown in Fig. 2) obtained from TD-DFT B3LYP/6-31G** calculations in gas phase and in ethanol. The absorption spectra of the studied compounds are characterized by a high molar absorptivity (40,000–45,000 M^{-1} cm^{-1}) and composite structure. The latter is more pronounced in a non-polar solvent like cyclohexane (not shown). Polar solvents cause slight bathochromic shift. Interestingly, however, the spectra in water are blue shifted by *ca.* 40 nm for **2**, **3** and **4**. The other compounds do not show this shift. In comparison with the absorption properties of 2-acetyl-1,3-indandione (2AID) the expected strong bathochromic shift for compounds **1**–**6** (due to the presence of elongated π-conjugation) is observed. Another structural parameter defining the position of the absorption maxima is the electron donating strength of the conjugated substituent as well as the planarity of the whole molecule. According to the DFT data, all studied compounds in their most stable conformation are very close to being completely planar; the largest dihedral angle between the plane of the 1,3-indandione fragment and that of the heterocyclic substituent is 0.07° for compound **2**. Comparing the absorption properties of compounds **1**–**6**, shown in Table 4, it can be concluded that molecular planarity, leading to a strong electron delocalization, is the main factor governing their optical properties.

The calculated vertical excitation energies of the most stable conformers of compounds **1**–**6** (TD-DFT B3LYP/6-31G**) in vacuum show a qualitative agreement with the experimental data, i.e., predicting higher excitation energy: the wavelength is reduced by *ca.* 30 nm compared to the experimental data. On the other hand, when including the solvent effects, the calculations give good agreement with the observed absorption maxima (Table 4, ethanol); the largest deviation (*ca.* 10 nm) is obtained for compounds **2**, **3** and **4**. Furthermore, TD-DFT calculations were performed for the optimized structures of the other possible rotamers and tautomers in gas phase. The results show that *cis–trans* isomerisations lead to small shifts in the vertical excitation energies (less than 10 nm) whereas keto–enol tautomerization results in drastic changes in the calculated excitation energies. Moreover, according to the gas-phase calculations tautomerization results in bathochromic shift of the long-wave-length band, by *ca.* 30 nm, and a similar shift but in the opposite direction of the other band. The former has only small oscillator strength, whereas the latter appears at about 330 nm and has much larger oscillator strength; ten times larger in compounds **2**, **3** and **4**. Such drastic changes in the experimental spectra, in six different solvents, were not observed except the strong hypsochromic shift seen in aqueous solution of compounds **2**, **3** and **4**. Poor solubility of all compounds in water, however, made a more detailed analysis not possible. The calculated energies of the **a** and **b** tautomers (Suppl. Mater.) do not show evidence for possible tautomerization. Further quantum-chemical calculations, explicitly taking account for the solvent effect, may reveal a possible tautomerization assisted by solvent molecules.

Another optical property that may give information on tautomerism is the emission spectrum. Steady-state fluorescence spectra were, therefore, recorded in three different solvents and it was found that they are characterized by a broad and structureless emission band. The estimated Stokes shift is about 100 nm (see Table 4), and the observed large Stokes shift (e.g. 125 nm for **1** in acetonitrile) suggests the occurrence of some intramolecular rearrangements in excited state. Similarly to the 2AID fluorescence, characterized by Stokes shift of 200 nm, the possibility of intramolecular proton transfer in the excited state of compound **1** was studied through theoretical calculations. We applied optimization procedure in which a single structural parameter was changed in small step in order to calculate the potential energy surface along the tautomerization or *cis–trans* isomerization process. The tautomerization was studied by changing the O3···H distance (see atom

Table 4
Absorption and emission properties of compounds **1–6** in various solvents (excitation wavelength is given in parentheses) compared with TD-DFT/B3YP-6-31G** calculation of vertical excitation energies in gas-phase and ethanol (in nm) and the corresponding oscillator strength – *f*.

Solvent	Acetonitrile		Absolute Ethanol		DMSO		TD-DFT vertical excitation (*f*)	
Comp.	λ_{abs}	λ_{emis}	λ_{abs}	λ_{emis}	λ_{abs}	λ_{emis}	Gas-phase	Ethanol
Comp. **1**	**371**, **385**	510 (385)	**372**, **385**	517 (380)	**378**, **391**, **410** sh	497 (390)	346.24 (1.04) 335.34 (0.15)	380.38 (1.17) 366.72 (0.19)
Comp. **2**	**412**	495 (410)	**413**	–	**410**	463 (405)	380.32 (1.01) 365.12 (0.13)	400.18 (1.22) 380.36 (0.07) 311.47 (0.09)
Comp. **3**	**390**	472 (390)	**373** sh, **390**, **409** sh	520 (390)	**379** sh, **396**, **415** sh	462 (400)	365.25 (0.41) 353.40 (0.82)	379.96 (0.88) 369.40 (0.51)
Comp. **4**	**408**	480 (410)	**409**, **426** sh	514 (410)	**399** sh, **416**, **437** sh	483 (415)	377.84 (0.74) 366.01 (0.46)	399.01 (1.10) 385.98 (0.23)
Comp. **5**	**365**, **380**, **400** sh	510 (380)	**364**, **379**	520 (380)	**371** sh, **385**, **406** sh	517 (370)	360.10 (0.90) 345.08 (0.26)	374.02 (1.21) 356.08 (0.13)
Comp. **6**	**365**, **380**, **401** sh	515 (380)	**364**, **380** sh	524 (365)	**371**, **386** **407** sh	520 (370)	360.40 (0.86) 349.03 (0.31)	373.27 (1.20) 357.81 (0.14)

sh – Shoulder.

numbering in Figs. 3a, 4a and 5a) from 0.900 to 1.700 Å, whereas for the *cis–trans* isomerization we varied the C8–C10–C11–C12 dihedral angle (see Fig. 6). These calculations were performed in the energetically lowest singlet and triplet states. To consider the energetically lowest triplet state instead of the first excited singlet, was used as an approximation that has successfully been applied for Stokes-shift calculation and motivated elsewhere [41]. For further confirmation of the applicability of this approximation, we performed analogous calculation for the tautomerization process in ground and excited triplet state for 2AID (show in Fig. 6), which has previously been studied by experimental and theoretical methods at the semiempirical level [11]. Our DFT calculation, with this approximation, are in agreement with the previous results for 2AID, showing that the relative stability of the **a** and **b** tautomers is different in the ground and the excited state, and thus explains the experimentally observed indication for ESIPT and its high photostability [12]. As can be seen from Fig. 6, the results for compound **1** show that in the ground and the excited state the relative stability of the studied tautomers is not reversed, i.e. in both states tautomer **a** is the most stable one. Similar results were obtained from calculations for the reaction coordinate for the *cis–trans* isomerization. These findings suggest that most probably the large Stokes shift is caused instead by strong charge redistribution taking place during the electronic transitions.

4. Conclusion

The structures of six 2-acyl-1,3-indandione derivates that posses intramolecular hydrogen bonding and extended π-electron conjugation, were determined in crystalline state and in gas phase using X-ray diffraction and quantum-chemical calculations, respectively. The results show that the molecular conformation in gas phase is the same like in solid state although C–C bond rotations are energetically allowed and despite the intermolecular interactions present in the crystal packing. This implies that the main component of stabilization energy of this series of compounds is the degree of π-electron delocalization between the 1,3-indandione fragment and the heterocyclic ring through the butadiene bridge. The optical (absorption) properties of the compounds were studied using both experimental and by theoretical methods, too. It was shown that the calculated vertical excitation energies are not sensitive to *cis–trans* isomerizations but differ considerably in the keto–enol tautomers. The calculated energy differences between both possible tautomers, however, are too large to allow tautomerization. Nevertheless, the spectra of compounds **2**, **3** and **4** in water show strong hypsochromic shift, expected for the **b** tautomer. To justify theoretically that tautomerization might take place in water would require a more accurate description of the process including an explicit treatment of the solvent molecules so that a proton transfer can be described. Our quantum-chemical calculations of the energetics along two possible reaction coordinates of compound **1** (tautomerization and rotamerization) in the ground and the energetically lowest triplet state show that the relative stability of the studied tautomers and rotamers is the same in both states. Thus, the experimentally observed strong Stokes shift of this compound could not be explained through intramolecular rearrangements in the excited state, in contrast to the case for 2AID, but is more likely caused by significant charge redistribution during the electronic transitions. Although the gas-phase calculations do not predict intramolecular rearrangements (tautomerization or rotamerizations) in the ground or excited state, the experimental data would require a more thorough theoretical description with an explicit description of the solvent molecules. This is, however, beyond the scope of the present work.

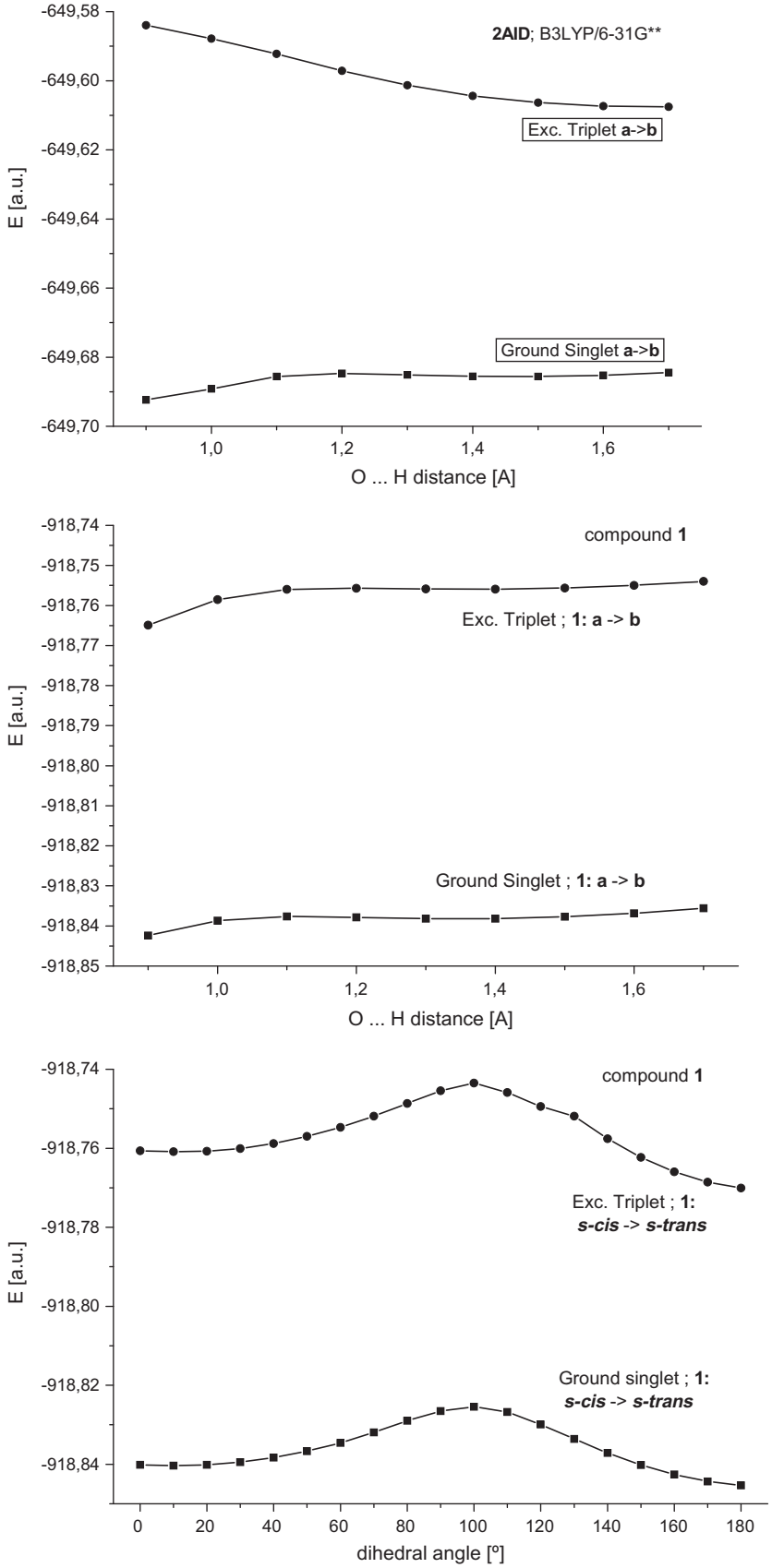

Fig. 6. Energy diagram for tautomerization (**a** → **b**) or *cis–trans* isomerization (**s-cis** → **s-trans**) processes for 2-acetyl-1,3-indandione (2AID) and compound **1** followed by B3LYP/6-31G** calculations in ground and excited triplet states.

Acknowledgements

The financial support from the National Science Fund of Bulgaria (Contract MYX-02/05) is gratefully acknowledged. The research was partially supported by the Ministry of Science and Technology of the Republic of Croatia (Grant No. 098-1191344-2943).

Appendix A. Supplementary material

CCDC numbers 775554–775556 for compounds **2**, **3** and **4**, respectively, contains the supplementary crystallographic data for this paper. These data can be obtained free of charge at www.ccdc.cam.ac.uk/conts/retrieving.html [or from the Cambridge Crystallographic Data Centre (CCDC), 12 Union Road, Cambridge CB2 1EZ, UK; fax: +44 (0) 1223 336033; email: deposit@ccdc.cam.ac.uk]. Structure factors table is available from the authors. Supplementary Material contains energy diagrams of all optimized conformers with B3LYP/6-31G** and HF/6-31G** of compounds **1**–**6** as well as a table listing the calculated total energies, ZPVE and energy differences. Supplementary data associated with this article can be found, in the online version, at doi:10.1016/j.molstruc.2010.07.008.

References

[1] M. Utinans, O. Neilands, Adv. Mater. Opt. Electr. 9 (1999) 19.
[2] P. Hrnciar, A. Gaplovsky, E. Jankulicova, J. Donovalova, Chem. Papers – Chem. Zvesti 42 (1988) 53.
[3] C. Bratschkov, S. Minchev, I. Schopov, Polymer 35 (1994) 1549.
[4] M.A. Tovmasyan, I.V. Bulgarovskaya, V.M. Vozzhennikov, Zh. Fiz. Khim. 58 (1984) 1428.
[5] M.A. Tovmasyan, I.V. Bulgarovskaya, V.M. Vozzhennikov, Zh. Fiz. Khim. 58 (1984) 1433.
[6] M. Mitewa, P.R. Bontchev, V. Enchev, S. Minchev, M. Kashchieva, J. Prakt. Chem. 327 (1985) 516.
[7] P.R. Bontchev, M. Mitewa, S. Minchev, M. Kashchieva, D. Mechandjiev, J. Prakt. Chem. 325 (1983) 803.
[8] V.A. Shagun, V.F. Sidorkin, V.A. Usov, M.G. Voronkov, Bull. Acad. Sci. USSR Div. Chem. Sci. 30 (1981) 1417.
[9] V. Enchev, I. Abrahams, G. Ivanova, J. Mol. Struct.: THEOCHEM 719 (2005) 169.
[10] P.N. Krishnan, L.A. Burke, J.O. Jensen, J. Mol. Struct.: THEOCHEM 305 (1994) 9.
[11] V. Enchev, S. Bakalova, G. Ivanova, N. Stoyanov, Chem. Phys. Lett. 314 (1999) 234.
[12] A. Ahmedova, V. Mantareva, V. Enchev, M. Mitewa, Int. J. Cosmetic Sci. 24 (2002) 103.
[13] A. Ahmedova, P. Marinova, S. Ciattini, N. Stoyanov, M. Springborg, M. Mitewa, Struct. Chem. 20 (2009) 101.
[14] A. Ahmedova, V. Atanasov, P. Marinova, N. Stoyanov, M. Mitewa, Cent. Eur. J. Chem. 7 (2009) 429.
[15] M. Sigalov, B. Shainyan, N. Chipanina, I. Ushakov, A. Shulunova, J. Phys. Org. Chem. 22 (2009) 1178.
[16] S. Jursenas, V. Gulbinas, Z. Kuprionis, R. Kananavicius, G. Kodis, T. Gustavsson, J.C. Mialocq, L. Valkunas, Synth. Met. 109 (2000) 169.
[17] V. Gulbinas, G. Kodis, S. Jursenas, L. Valkunas, A. Gruodis, J.C. Mialocq, S. Pommeret, T. Gustavsson, J. Phys. Chem. A 103 (1999) 3969.
[18] S. Jursenas, V. Gulbinas, A. Gruodis, G. Kodis, V. Kovalevskij, L. Valkunas, Phys. Chem. Chem. Phys. 1 (1999) 1715.
[19] S. Jursenas, A. Gruodis, G. Kodis, M. Chachisvilis, V. Gulbinas, E.A. Silinsh, J. Phys. Chem. B 102 (1998) 1086.
[20] H. Schwartz, R. Mazor, V. Khodorkovsky, L. Shapiro, J.T. Klug, E. Kovalev, G. Meshulam, G. Berkovic, Z. Kotler, S. Efrima, J. Phys. Chem. B 105 (2001) 5914.
[21] N.S. Saleesh Kumar, S. Varghese, C.H. Suresh, N.P. Rath, S. Das, J. Phys. Chem. C 113 (2009) 11927.
[22] Oxford Diffraction Ltd., Xcalibur CCD system, CrysAlis Software system, Version 1.171.32.29. Abingdon, Oxfordshire, England, 2008.
[23] G.M. Sheldrick, Acta Cryst. A64 (2008) 112.
[24] L.J. Farrugia, J. Appl. Cryst. 32 (1999) 837.
[25] L.J. Farrugia, J. Appl. Cryst. 30 (1997) 565.
[26] L. Spek, J. Appl. Cryst. 36 (2003) 7.
[27] C.F. Macrae, I.J. Bruno, J.A. Chisholm, P.R. Edgington, P. McCabe, E. Pidcock, L. Rodriguez-Monge, R. Taylor, J. van de Streek, P.A. Wood, J. Appl. Cryst. 41 (2008) 466.
[28] A.D. Becke, J. Chem. Phys. 98 (1993) 5648.
[29] S. Lee, W. Yang, R.G. Parr, Phys. Rev. B 37 (1998) 785.
[30] M.J. Frisch, G.W. Trucks, H.B. Schlegel, G.E. Scuseria, M.A. Robb, J.R. Cheeseman, J.A. Montgomery, Jr., T. Vreven, K.N. Kudin, J.C. Burant, J.M. Millam, S.S. Iyengar, J. Tomasi, V. Barone, B. Mennucci, M. Cossi, G. Scalmani, N. Rega, G.A. Petersson, H. Nakatsuji, M. Hada, M. Ehara, K. Toyota, R. Fukuda, J. Hasegawa, M. Ishida, T. Nakajima, Y. Honda, O. Kitao, H. Nakai, M. Klene, X. Li, J.E. Knox, H.P. Hratchian, J.B. Cross, V. Bakken, C. Adamo, J. Jaramillo, R. Gomperts, R.E. Stratmann, O. Yazyev, A.J. Austin, R. Cammi, C. Pomelli, J.W. Ochterski, P.Y. Ayala, K. Morokuma, G.A. Voth, P. Salvador, J.J. Dannenberg, V.G. Zakrzewski, S. Dapprich, A.D. Daniels, M. C. Strain, O. Farkas, D.K. Malick, A.D. Rabuck, K. Raghavachari, J.B. Foresman, J.V. Ortiz, Q. Cui, A.G. Baboul, S. Clifford, J. Cioslowski, B.B. Stefanov, G. Liu, A. Liashenko, P. Piskorz, I. Komaromi, R.L. Martin, D.J. Fox, T. Keith, M.A. Al-Laham, C. Y. Peng, A. Nanayakkara, M. Challacombe, P.M.W. Gill, B. Johnson, W. Chen, M.W. Wong, C. Gonzalez, J.A. Pople, Gaussian, Inc., Pittsburgh PA, Gaussian 03, Revision B.03, 2003.
[31] A. Ahmedova, G. Pavlović, D. Šišak, M. Mitewa, Unpublished results.
[32] G. Gilli, F. Bellucci, V. Ferretti, V. Bertolasi, J. Am. Chem. Soc. 11 (1989) 1023.
[33] P. Gilli, V. Bertolasi, V. Feretti, G. Gilli, J. Am. Chem. Soc. 116 (1994) 909.
[34] F.H. Allen, O. Kennard, D.G. Watson, L. Brammer, A.G. Orpen, R. Taylor, J. Chem. Soc. Perkin Trans. II (1987) S1.
[35] I. Csoregh, R. Norrestam, Acta Crystallogr. B 32 (1976) 2450.
[36] J.D. Korp, I. Bernal, T.L. Lemke, Acta Cryst. B 36 (1980) 426.
[37] J.G. Garcia, J.D. Enas, Acta Cryst. C49 (1993) 1823.
[38] C.A. Hunter, J.K.M. Sanders, J. Am. Chem. Soc. 112 (1990) 5525.
[39] M.D. Curtis, J. Cao, J.W. Kampf, J. Am. Chem. Soc. 126 (2004) 4318.
[40] C.A. Hunter, Chem. Soc. Rev. 23 (1994) 101.
[41] O. Clemens, M. Basters, M. Wild, S. Wilbrand, C. Reichert, M. Bauer, M. Springborg, G. Jung, J. Mol. Struct.: THEOCHEM 866 (2008) 15.